Batteries & Supercaps

Research Article
doi.org/10.1002/batt.202200167

Chemistry Europe
European Chemical Societies Publishing

www.batteries-supercaps.org

VIP *Very Important Paper*

Special Collection

Graphene-based Activated Carbon Composites for High Performance Lithium-Sulfur Batteries

Gonzalo Jiménez-Martín,[a, b] Julen Castillo,[a, b] Xabier Judez,*[a] Juan Luis Gómez-Urbano,[a, b] Gelines Moreno-Fernández,[a] Alexander Santiago,[a] Amaia Saenz de Buruaga,[a] Iñigo Garbayo,[a] Jose Antonio Coca-Clemente,[a] Aitor Villaverde,[a] Michel Armand,[a] Chunmei Li,*[a] and Daniel Carriazo[a, c]

The increasing demand for electrical energy storage requires the exploration of alternative battery chemistries that overcome the limitations of the current state-of-the-art lithium-ion batteries. In this scenario, lithium-sulfur batteries stand out for their high theoretical energy density. However, several inherent limitations still hinder their commercialization. In this work, we report the synthesis and study of two high-performance activated carbon-based materials that allow to overcome the most challenging limitations of sulfur electrodes, i.e., low electronic conductivity and the polysulfide shuttle effect. The two tailored nanomaterials are based on porous carbon structures mixed with conductive reduced graphene oxide, one derived from an organic waste and the other from an organic synthetic route. These structures not only feature excellent individual properties, but also present excellent performance when implemented in batteries, related to their superior conductivity and polysulfide trapping ability, allowing to obtain improved rate capacity and high sulfur loading cycling. Additionally, we demonstrate the scalability of the best performing material by the assembly of high-performance pouch cells.

Introduction

Driven by technological evolution, batteries have been developed to provide power for a diverse range of applications, from microchips to electric vehicles. Several battery chemistries have been deployed so far, and over the last 3 decades, lithium-ion batteries (LIBs) have become the most advanced electrochemical energy storage technology and billions of units have been produced.[1,2] However, despite the recent advances, the properties of these batteries fall behind the tightly demanding key performance indicators of new technologies, such as electric vehicles.[3] Therefore, alternative battery chemistries have been explored with the aim of improving the energy density of the LIBs.[4] Among them, lithium-sulfur batteries (LSBs) stand out driven by the low cost, environmental friendliness, and high theoretical capacity of the sulfur active material (1675 $mAh\,g^{-1}$), enabling energy densities of over 400 $Wh\,kg^{-1}$.[5] These characteristics make LSBs really appealing for lightweight applications. However, the practical performance of LSBs is impeded by several issues, including i) low conductivity and large volume changes from S_8 to the final discharge product Li_2S, causing low sulfur utilization and compromising structural integrity of the cathode; ii) dissolution and diffusion of reaction intermediates [i.e., lithium polysulfides (LiPS), Li_2S_x, $x = 8, 6, 4, 2$], which poison the anode, in the so-called "polysulfide shuttle effect"; and iii) the challenge of using of metallic lithium, related to its high reactivity and the generation of lithium dendrites.[6,7]

Several strategies have emerged during the last two decades to overcome these limitations, with a special focus on the properties and design of the sulfur cathode.[8] The cathodes usually comprise sulfur as active material, a conductive carbon that allows a continuous flow of electrons to the sulfur surface, and a polymeric binder that agglutinates electrode components among them and to the aluminum current collector. Besides the electron conducting role, carbons play a key role to buffer volume changes of electroactive materials, and to act as polysulfide anchors via physical barriers or chemical interaction.[9] Therefore, carbons with diverse properties have been intensively explored for LSBs.[10]

Porous carbons with high surface area and *ad-hoc* pore size are the most common choice for LSBs.[11] These carbons can accommodate high loadings of sulfur in a conductive network, accommodate its volume expansion, and up to some extent,

[a] G. Jiménez-Martín, J. Castillo, Dr. X. Judez, Dr. J. L. Gómez-Urbano, Dr. G. Moreno-Fernández, Dr. A. Santiago, A. Saenz de Buruaga, Dr. I. Garbayo, Dr. J. A. Coca-Clemente, A. Villaverde, Prof. M. Armand, Dr. C. Li, Dr. D. Carriazo
Centre for Cooperative Research on Alternative Energies (CIC EnergiGUNE), Basque Research and Technology Alliance (BRTA)
01510 Vitoria-Gasteiz, Spain
E-mail: xjudez@cicenergigune.com
cli@cicenergigune.com
[b] G. Jiménez-Martín, J. Castillo, Dr. J. L. Gómez-Urbano
University of the Basque Country (UPV/EHU)
Barrio Sarriena, s/n, 48940 Leioa, Spain
[c] Dr. D. Carriazo
IKERBASQUE, Basque Foundation for Science
48013 Bilbao, Spain

Supporting information for this article is available on the WWW under https://doi.org/10.1002/batt.202200167

Special Collection *An invited contribution to a Special Collection dedicated to Lithium–Sulfur Batteries*

Research Article
doi.org/10.1002/batt.202200167
Chemistry Europe
European Chemical Societies Publishing

trap LiPSs.[10,12] For this purpose, Ketjenblack® EC-600JD (KJ600) has been widely used due to its high surface area of ~1400 $m^2 g^{-1}$ and commercial availability.[13–16] However, KJ600 presents unsatisfactory electronic conductivity for high sulfur utilization, especially with high loading at fast C-rates. Additionally, the structure of KJ600 is mainly formed by big micropores and mesopores, which are not the most adequate for LiPS retention.[17,18] Thus, the exploration of novel porous carbon nanostructures with tailored properties is an appealing strategy for the development of LSBs.

In addition, the incorporation of nanostructured materials to the electrode formulation is as well considered as a promising solution to improve the low conductivity of sulfur.[19] Among them, graphene, a bidimensional material composed by carbon atoms in a single layer honeycomb lattice, has attracted considerable attention. Graphene-based materials employed for this purpose are generally based on reduced graphene oxide (rGO), due to its optimum conductivity.[18] These materials present excellent mechanical properties and wettability that improve the diffusion of the electrolyte into the microstructure of the electrode.[9,20]

Consequently, the synthesis of novel porous carbon composites combining activated carbons (ACs) within rGO is an appealing strategy that will help to overcome the most limiting issues of LSBs. For that purpose, we report the synthesis, characterization, integration into a sulfur cathode and electrochemical study of two novel carbons. Two different sources are employed for the fabrication of these ACs. On one hand, coffee-waste is used in combination with graphene oxide (GO) for the fabrication of the so-called rGOCaf AC. On the other hand, the second AC is prepared through resorcinol/formaldehyde condensation in the presence of GO for the fabrication of ResFArGO (see the Experimental Section for further details). This paper not only presents the study of two in-house materials for LSBs for the first time, but also demonstrates the suitability of our novel nanoscale materials for improving the performance of LSBs in practical working conditions (up to 4 $mg_S cm^{-2}$). Furthermore, we also demonstrate the scalability of our nanoscale materials by the implementation of the best one at pouch cell level.

Results and Discussion

As previously described, this work focuses on the evaluation of different graphene-based ACs as suitable sulfur hosts for their utilization in high-sulfur loading LSB cathodes. The two in-house ACs, i.e., ResFArGO and rGOCaf, were fabricated from different sources, as mentioned in the previous paragraph and detailed in the Experimental Section. For the sake of comparison KJ600, a commercial AC, is also evaluated.

Figure 1 presents the structural properties of commercial KJ600 and in-house produced rGOCaf and ResFArGO carbons. The SEM images in Figure 1(a–c) show big differences in particle morphology. Commercial AC (KJ600, Figure 1a) is formed by submicrometer-sized irregularly shaped particles with a non-uniform distribution. In contrast, graphene-coffee waste derived AC (rGOCaf, Figure 1b) shows larger particle sizes, which are characteristic of biowaste-derived carbons,[21] but homogenously coated by rGO sheets, the product of the thermal reduction of GO. ResFArGO (Figure 1c) presents an open and uniform flat-shaped structure, consisting of homogenously distributed AC flakes. This bidimensional structure is ascribed to the templating effect of GO during the hydrothermal polycondensation of resorcinol.[22] In both cases, graphene-containing ACs present open structures that will allow to buffer the volume changes during cycling and at the same time could serve as LiPS reservoirs; in contrast to KJ600, which presents a much more compact structure.

Textural properties of the carbons were further studied by nitrogen adsorption/desorption isotherms at −196 °C. Figure 1d shows that the different ACs feature different profile types according to IUPAC classification.[23] KJ600 isotherm presents a type-IV profile, characteristic of mesoporous materials. In addition, its type H3 hysteresis loop can be assigned to aggregates of plate-like particles giving rise to slit-shaped pores.[24] On the other hand, while rGOCaf shows a mixture of type-I and IV isotherms, combining micropores with a small contribution of mesopores, ResFarGO profile can be indexed as a type-I, characteristic of microporous materials. It is worth to remark that graphene-containing ACs show higher BET specific surface areas (2350 and 2318 $m^2 g^{-1}$ for rGOCaf and ResFArGO, respectively) when compared to that of the commercial KJ600 (1383 $m^2 g^{-1}$). Pore size distributions (PSDs) calculated from the isotherms are depicted in Figure 1(e). While KJ600 has an uneven PSD, including micropores (~1 nm) and mesopores (~5 nm); a narrower micropore size distribution is displayed for the graphene-containing samples. Even though, as predicted from the shape of the isotherm, rGOCaf has wider micropores than that of ResFArGO. To sum up, both prepared carbons feature increased surface areas and a narrower distribution of smaller size pores compared to commercial KJ600.

Afterwards, to prepare sulfur@carbon composites, sulfur was infiltrated in the AC structures, by a melt diffusion process at 155 °C for 12 h to obtain the hereafter referred to as "S@AC composites". The SEM images of the three different S@C are shown in Figure 2(a–c). SEM image of S@KJ600 composite (Figure 2a) suggests an enlarged particle size when compared to that of pristine KJ600 (Figure 1a) which could be ascribed to the agglomeration of the carbon particles due to the incorporation of sulfur in the composite. In contrast, the SEM images of the graphene-based composites (Figure 2b and c) show that the deposition of sulfur does not produce any significant structural change with respect to sulfur-free ACs (Figure 1b and c). Moreover, the absence of sulfur agglomerates suggests that sulfur has been homogeneously distributed along the surface of the ACs. XRD patterns in Figure S1(a) confirm the integration of sulfur in the composites. The XRD patterns of pristine S_8 (JCPDS No. 08-0247) show well-defined and highly intense diffraction peaks, due to the crystalline nature of orthorhombic sulfur. However, when sulfur is infiltrated in the different carbons, those peaks are clearly abated due to the strong sulfur storing properties of the carbons and the total dispersion of sulfur into the pores of the ACs.[25,26] The Raman spectra

Research Article
doi.org/10.1002/batt.202200167
Chemistry Europe
European Chemical Societies Publishing

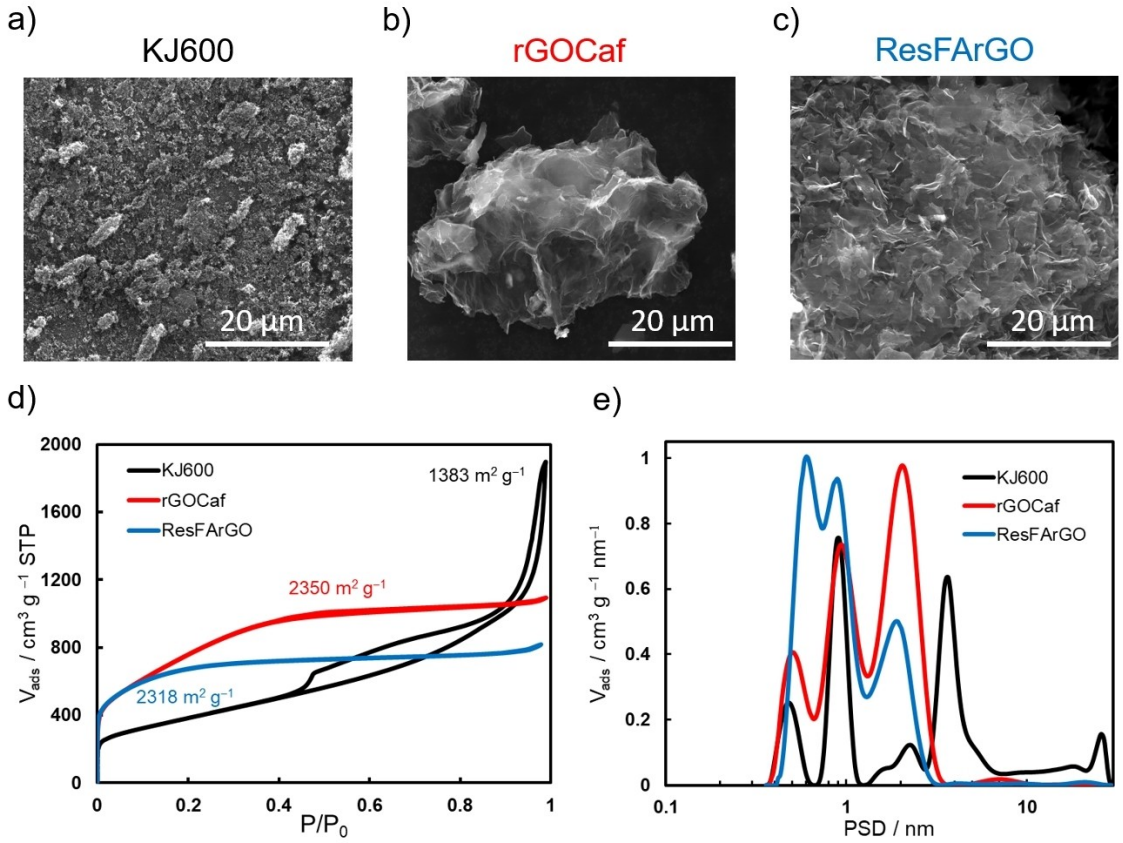

Figure 1. a–c) SEM images, d) N_2 adsorption-desorption isotherms, and e) calculated pore size distributions of KJ600, rGOCaf and ResFArGO activated carbons.

registered for these materials further confirm the presence of the carbonaceous matrix in the composites (Figure S1b). Two broad Raman peaks observed at ~1330 and 1600 cm^{-1}, respectively, are assigned to the G and D bands of graphite. G-band could be ascribed to sp^2 carbon vibration while the D-band could be associated to dispersive, defect induced vibrations, due to the disordered structure of the graphene sheets. The value of the ratio between the integrated areas of the D-band (A_D) and G-band (A_G) are 1.89, 1.52 and 1.52 for S@KJ600, S@rGOCaf and S@ResFArGO respectively, indicating a lower concentration of defects and a larger degree of graphitization for the graphene containing samples.[21] The absence of sulfur peaks in the Raman spectra suggests that crystalline sulfur clusters are homogeneously dispersed along the graphene surface.[27,28]

As indicated in the Introduction, the LiPS shuttle effect is one of the biggest challenges for LSBs battery development. However, the migration of the LiPS can be effectively limited by its adsorption in carbon structures. Therefore, it is necessary to analyze the LiPS adsorption capability of the carbon structures in order to assess their suitability for LSBs. The visual test shown in Figure 2 (d) demonstrates huge differences in LiPS adsorption capabilities depending on the different carbonaceous matrix employed. KJ600 is the less prone carbon to adsorb LiPS, while the two in-house materials decrease more prominently the coloration of the solution. This is related to the higher surface area and smaller pore sizes of our materials in comparison with KJ600,[29] and as well could be related to the remaining functional groups from GO that can serve as anchor sites for the efficient trapping of the high order LiPS. Additionally, amongst our two carbons, ResFArGO sample demonstrates higher adsorption capability than rGOCaf. Even if they have a similar surface area, the difference is related to the narrower average pore size of ResFArGO, which makes it more suitable for LiPS retention.[18]

Finally, positive sulfur electrodes containing different carbons were fabricated by simple magnetic stirring of cathode materials in water, as described in the Experimental Section. The morphology of high sulfur loading cathodes (~4 $mg_S\,cm^{-2}$) is evaluated in Figure 3. Optical image in Figure 3(a) shows a very poor material adhesion along with cracks evolution in the surface of S@KJ600 electrodes. This could be related to the propensity of KJ600 to form agglomerates after S_8 addition. In contrast, with both S@rGOCaf (Figure 3b) and S@ResFArGO (Figure 3c) carbons, excellent material attachment and a homogeneous material distribution are obtained. SEM image in Figure 3(d) confirms the existence of micron-size cracks in S@KJ600 electrodes, while such defects are not visible in the electrodes containing graphene-based ACs (Figure 3e and f). Furthermore, S@rGOCaf and S@ResFArGO electrodes present excellent particle distribution, with no visible agglomeration. This confirms the excellent packing

Research Article
doi.org/10.1002/batt.202200167
Chemistry Europe
European Chemical Societies Publishing

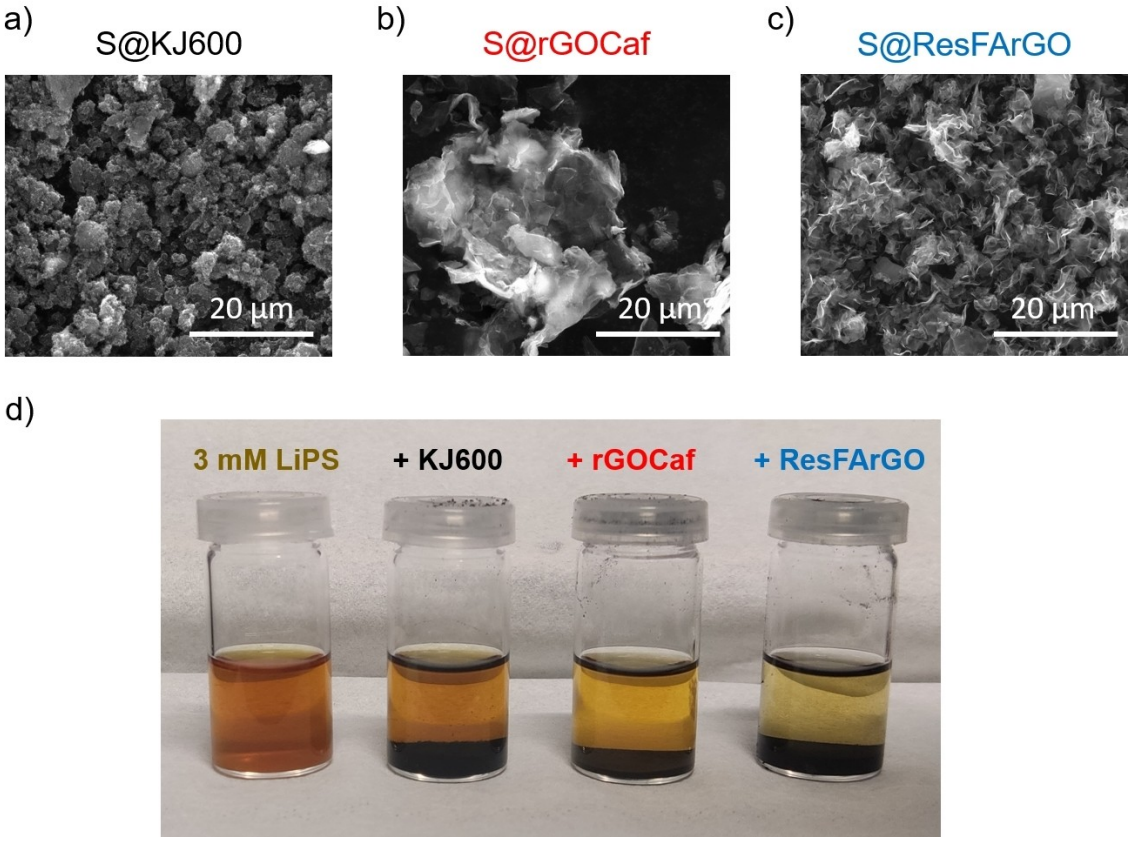

Figure 2. a–c) SEM images of the S@AC composites and d) LiPS adsorption test for the different ACs.

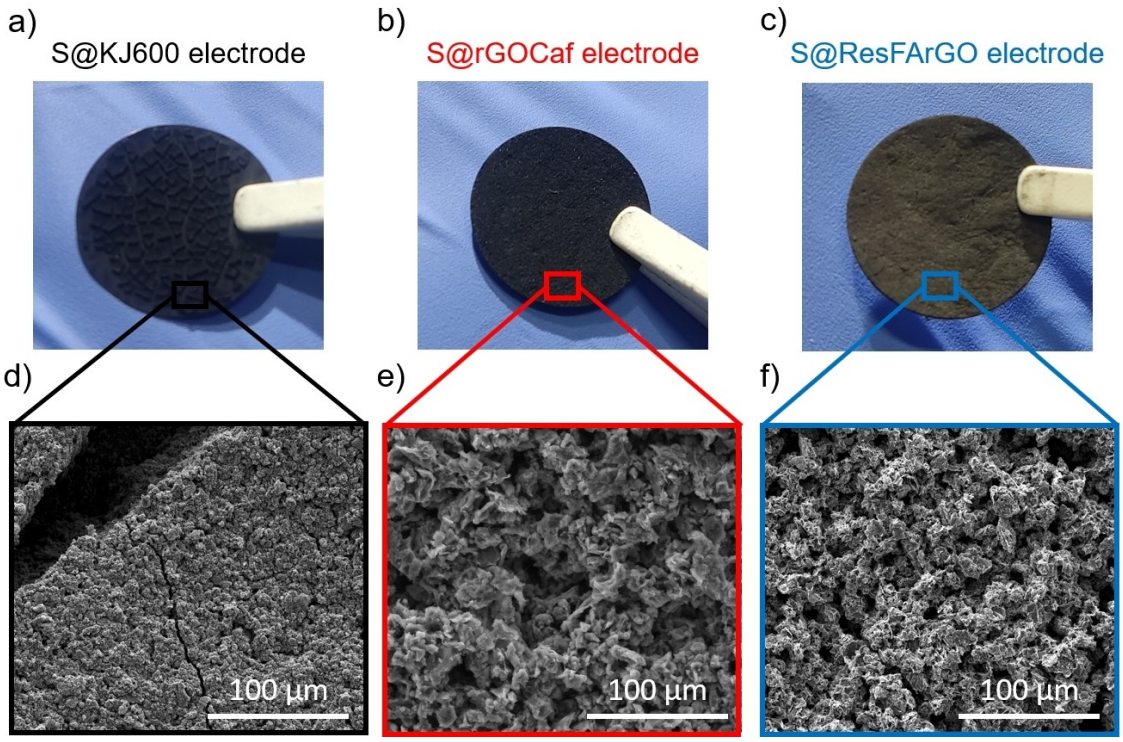

Figure 3. a–c) Optical images and d–f) SEM images of the prepared high sulfur loading electrodes with the three different carbon samples.

Research Article
doi.org/10.1002/batt.202200167
Chemistry Europe
European Chemical Societies Publishing

properties of our carbons and their suitability for the fabrication of high sulfur loading electrodes.

The electrochemical performance of the S@ACs was tested under various conditions in Figure 4. Medium loading cells ($\approx$2.5 $mg_S\,cm^{-2}$) underwent galvanostatic cycling at different C-rates, including C/20, C/10, C/5 and C/2. Gravimetric and areal capacity plots of the assembled cells are shown in Figure 4 (a and b), respectively. Both rGOCaf and ResFArGO cells displayed higher specific and areal capacities in the whole range of current densities in comparison with the cells assembled with commercial KJ600 as sulfur host. Moreover, graphene containing cathodes demonstrated outstanding capacity retention when C-rate is increased from C/10 to C/2 (73% for rGOCaf and 89% for ResFArGO). This could be related to the excellent attributes of the in-house ACs that combine high specific surface area for sulfur conversion reaction and LiPS retention, with high electronic conductivity from rGO sheets that allows formidable response to fast cycling. Remarkably, the S@ResFArGO cathode outstands with the best rate response, delivering capacities of 950 mAh g^{-1} (2.50 mAh cm^{-2}) at a high rate of C/2, with a very polarization at high currents, as shown in discharge/charge profiles in Figure 4(c). It is worth mentioning that S@ResFArGO cell is highly stable, with coulombic efficiencies over 99.8% at all the tested rates. Discharge/charge profiles for S@KJ600 and S@rGOCaf are included in Figure S2, where a small polarization is observed for S@rGOCaf, whilst remarkably higher polarization is observed for reference S@KJ600 system, with observable voltage shifts at C/10 and higher cycling rates.

Cyclability tests were performed with high loading cells (~4 $mg_S\,cm^{-2}$) at a constant rate of C/10 (after 5 formation cycles at C/20) (Figure 4d and e). Here, again, both graphene-based electrodes feature remarkably improved capacity of 780 mAh g^{-1} (2.96 mAh cm^{-2}) for S@rGOCaf and 1100 mAh g^{-1} (3.90 mAh cm^{-2}) for S@ResFArGO, in comparison with a low capacity of 520 mAh g^{-1} (1.80 mAh cm^{-2}) for reference S@KJ600. Again, S@ResFArGO cell stands out for obtaining the highest capacity and a very stable cycling (capacity retention of >99.7% from the first to the last cycle at C/10), with almost unaltered discharge/charge profiles along 50 cycles (Figure 4f). Disharge/charge profiles of S@KJ600 and S@rGOCaf are included in Figure S3 for comparison. S@rGOCaf cell presents some erratic charges before cycle 40 derived from lithium instability and probably due to some mild LiPS attack at the anode. This phenomenon is less aggressive in the S@KJ600 cell because the lower cell capacity derives in a milder cycling of the lithium anode and less LiPS generation. Taking the aforementioned into account, the S@ResFArGO cell also presents the best electrochemical performance in terms of long cycle life, specific capacity and areal capacity.

In order to identify the failure mechanism of the cells, *post-mortem* analysis of high loading cells have been carried out at the end of their cycle life. Optical images of the individual cell components are shown in Figure 5. Cathodes and anodes were recovered, washed with DME, and then evaluated by SEM imaging (Figure S4). Cathode image of S@KJ600 cell in Figure 5 shows a fractured electrode, with active material peeling off from the current collector. Some active material is adhered to the separator, which shows coloration due to the presence of

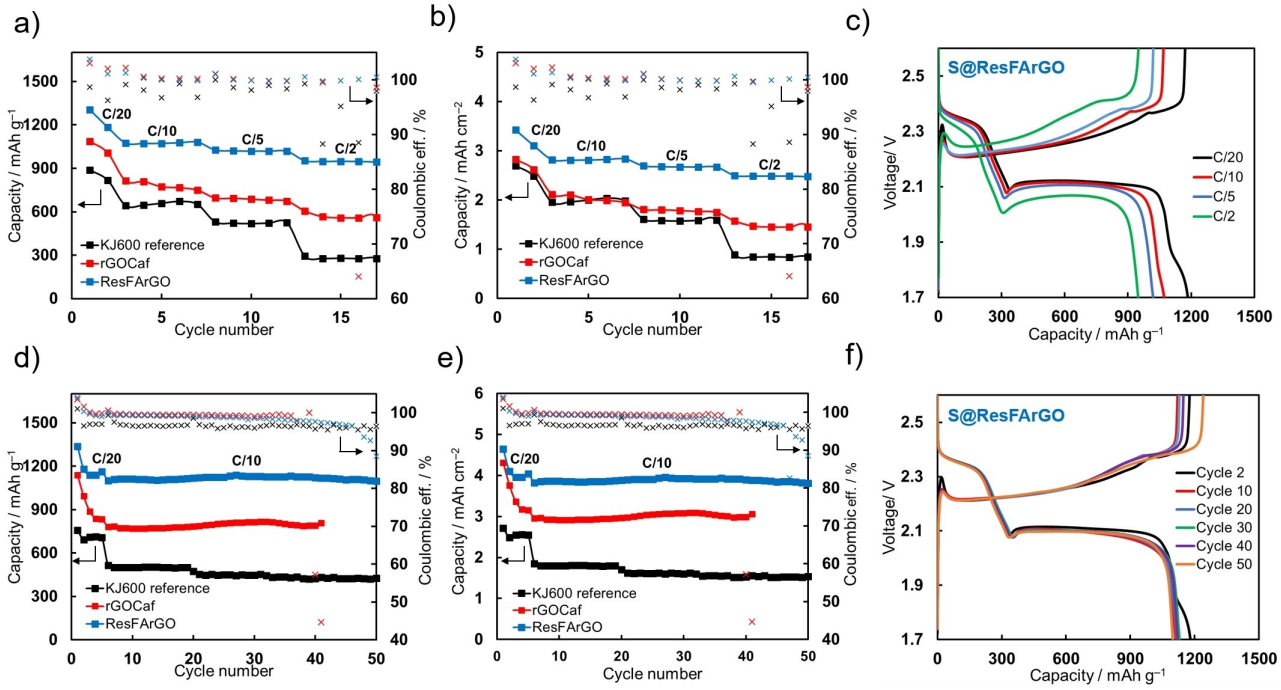

Figure 4. Galvanostatic cycling tests at coin cell level of the different electrodes. a) Gravimetric and b) areal capacities of medium sulfur loading cells at different capacities for noted electrodes, along with c) corresponding discharge/charge profiles for S@ResFArGO cell. d) Gravimetric and e) areal capacities of high sulfur loading cells at C/20 (5 cycles) and C/10 and the three studied carbons, along with f) corresponding discharge/charge profiles for S@ResFArGO cell.

Research Article
doi.org/10.1002/batt.202200167
Chemistry Europe
European Chemical Societies Publishing

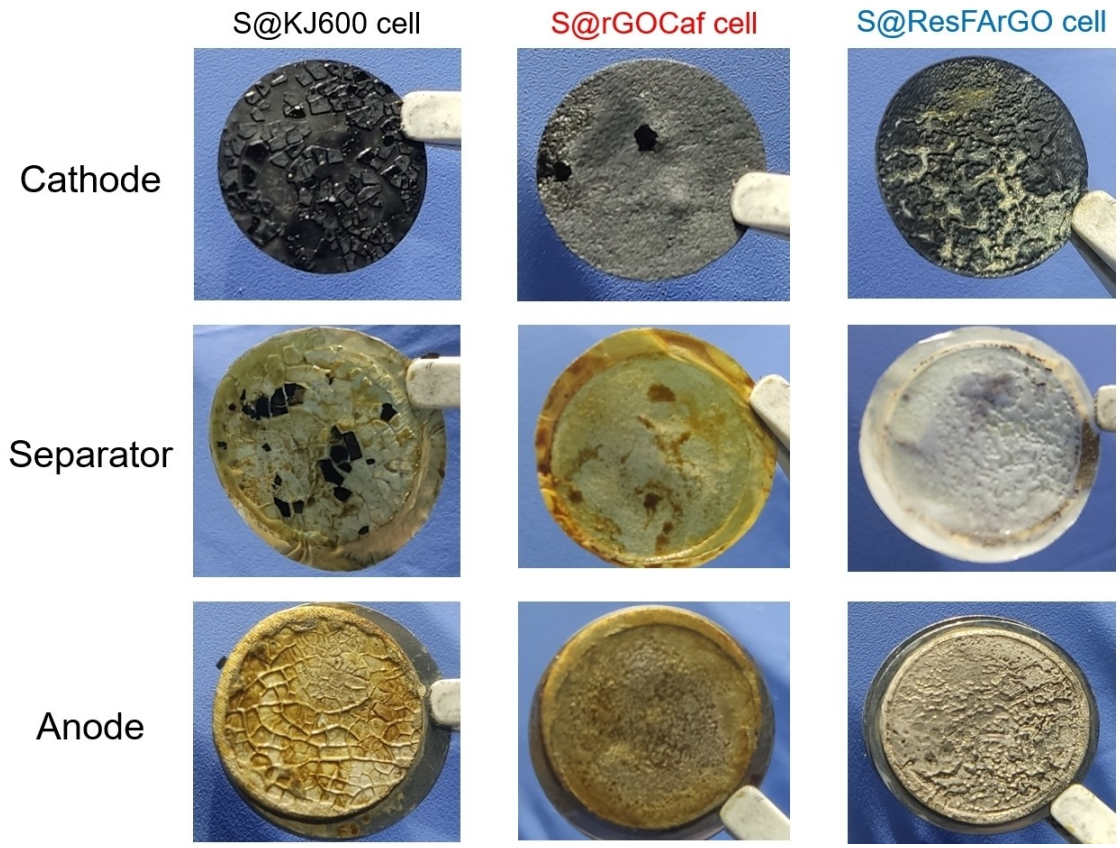

Figure 5. Optical images of the cathode, separator and anode of high loading cells at the end of their cycling life for the three carbon composites.

dissolved LiPS in the electrolyte. The collapse of the cathode and the presence of soluble LiPS explain the low capacity of the corresponding cell.

In contrast, the structural integrity of both S@rGOCaf and S@ResFArGO cycled cathodes was maintained after 40–50 cycles, as confirmed also by SEM images in Figure S4(a). The main difference between both systems is that while in S@rGOCaf cell there is a strong coloration due to the presence of dissolved LiPS, S@ResFArGO cell remains unaltered. Remarkably, despite the highest capacity obtained in this cell, the separator does not have any orange color after 50 cycles. Meanwhile, sulfur remains deposited at the surface of the ResFArGO cathode, which allows its further utilization leading to high sulfur utilization and capacity retention. Finally, the lithium anode seems to be damaged in both systems, as confirmed in the SEM images (Figure S4b). Therefore, we ascribe the long-term cell failure in S@ResFArGO system mainly to anode failure at such high areal capacities, while we believe the failure cause is the same in S@rGOCaf cell, but accelerated by the presence of partially dissolved LiPS.

In view of the results, S@ResFArGO composite was selected for its further evaluation in a 20 cm^2 pouch cell configuration. Figure 6(a) shows the size of the upscaled S@ResFArGO electrode and pouch cell, whose area is more than 15 times bigger than in coin cell configuration. Figure 6b shows the gravimetric capacities of S@ResFArGO pouch cell, demonstrating a comparable sulfur utilization to that obtained in the coin cell configuration (i.e., 1200 mAh g^{-1} and 3.5 mAh cm^{-2}). The corresponding areal capacities and discharge/charge profiles shown in Figure S5 confirm the excellent electrochemical response of the upscaled electrode. This demonstrates scalability of our material and its suitability for high performance in realistic working conditions. We must point out that, as indicated by other works, long-term stability issues related with the instability of lithium anode are more prominent in pouch cell, due to the significantly higher total current passed in the electrode.[30–32] This effect is visible after opening the pouch cell at the end of cycling life (Figure S6). Mossy and dead Li formed upon cycling and Li metal became sandy, which critically limits the lifespan of S@ResFArGO pouch cells. Therefore, after solving the major issues in the cathode by the implementation of new generation ResFArGO carbons, future studies focusing on Li anode protection are crucial, however are out of scope of this study.

Conclusion

In conclusion, we report the synthesis and the study of two carbonaceous materials consisting of the combination of AC hosts and highly conductive rGO, i.e., rGOCaf and ResFArGO. Those materials not only present excellent individual properties, such as high surface area and optimum pore size, but also feature excellent compatibility with sulfur, resulting in electro-

Research Article
doi.org/10.1002/batt.202200167
Chemistry Europe
European Chemical Societies Publishing

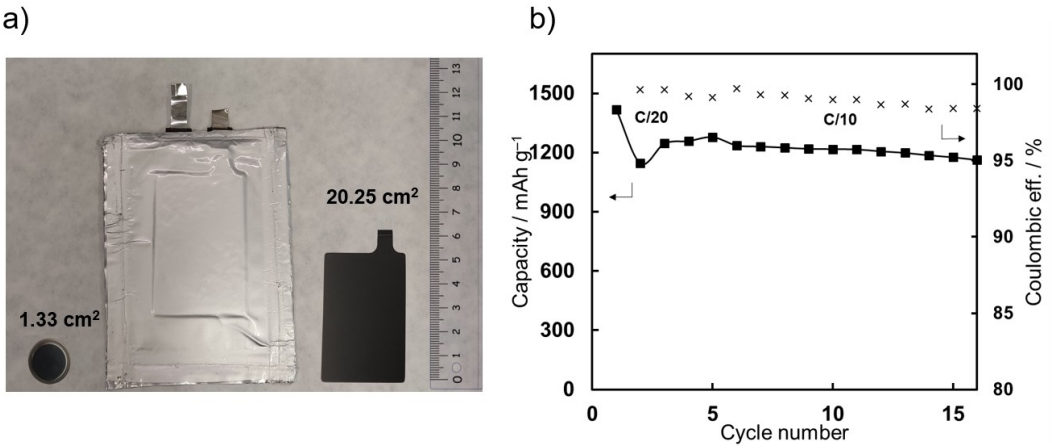

Figure 6. a) Optical images of the S@ResFArGO coin size and pouch size cathodes, along with the corresponding pouch cell. b) Gravimetric capacities of S@ResFArGO pouch cells at C/20 (2 cycles) and C/10.

des with excellent electrochemical properties. The presence of graphene and small micropores enables high electronic conductivity and trapping effect of LiPS. This brings great benefit, especially for the Li–S cells containing ResFArGO, which provide outstanding capacity of above 1100 mAh g^{-1} at high S loadings of 4 $mg_s\,cm^{-2}$, and a great C-rate respond. This study demonstrates that ACs with high surface areas and small micropores feature excellent electrochemical performance in Li–S electrodes.

Finally, due to its excellent performance, we demonstrate the scalability and practical application of this tailored nanomaterial by the preparation of 20 cm^2 pouch cell electrodes, which provided very high sulfur utilization. In this work we demonstrate that the main cathode challenges can be solved with the incorporation of ResFArGO carbon, whilst the use of high current densities will be challenging for the lithium anode. Post-mortem analysis has suggested that the degradation of Li metal anode (mossy and dead Li) is the main reason for the short cycle life of the cells. Further work should overcome this issue in order to improve the cycle life.

Experimental Section

Material and electrode preparation: rGOCaf synthesis was done following the procedure from our team.[21] In brief, dried coffee waste and graphene oxide dispersion (Graphene, 4 mg mL^{-1}) were vigorously stirred. The suspension was then freeze-dried, and precarbonized in a tubular oven at 400 °C under dynamic Ar atmosphere. Then, the carbon was activated by reaction with KOH (≥85 wt.%, Sigma Aldrich) in a ratio of 1:6 (C:KOH, wt.:wt.) at 800 °C under Ar atmosphere. The activated carbons were washed first using 6% v.% water solution of HCl (37 wt.%, Scharlab) and then several times after with hot deionized water. Dry powder was obtained after freeze-drying the material.

For the preparation of ResFArGO, details can also be found in the previous work from our group.[22] In this case, resorcinol (99 wt.%, Sigma Aldrich) was initially dissolved in water and ethanol, and then graphene oxide dispersion was added and vigorously stirred. Afterwards, formaldehyde (37 wt.%, Sigma Aldrich) and phosphoric acid catalyst (≥85 wt.%, Sigma Aldrich) were added at once and the mixture was transferred in closed recipients to an oven at 85 °C for 70 h to conduct the hydrothermal condensation. The obtained resins were heated at 800 °C in a tubular oven under Ar atmosphere to obtain the carbon. Finally, the carbon was activated, washed and dried following the same steps as in rGOCaf synthesis.

Positive electrodes were prepared with a final composition of 64 wt.% sulfur (≥99 wt.%, Sigma Aldrich), 26 wt.% carbon and 10 wt.% CMC (Sigma Aldrich)/SBR (Jingrui). Sulfur was initially infiltrated into carbon by melt diffusion at 155 °C for 12 h. Studied carbons were KetjenBlack® (EC-600JD, Akzo Nobel) (KJ600) as benchmark, and rGOCaf and ResFArGO as novel in-house materials. In parallel, CMC was magnetically stirred in water until it was totally dissolved. After, C@S powders were added and vigorously stirred for 4 h. Finally, SBR solution was added, and magnetically stirred for 24 h. Resulting slurries were coated on carbon coated aluminum foil fixing the sulfur loading at 2.5 $mg_s\,cm^{-2}$ for medium loading electrodes and 4 $mg_s\,cm^{-2}$ for high loading ones. The electrodes were gently dried initially at RT to avoid cracking and vacuum-dried later at 50 °C overnight. Finally, electrodes of 13 mm diameter or 37.5×54 mm were punched for coin cell assembly or pouch cell assembly, respectively. For pouch cell assembly, ResFArGO/S electrodes with a sulfur loading of 3 $mg_s\,cm^{-2}$ were used.

Characterization: The morphology of the materials and the electrodes was analyzed by scanning electron microscopy (SEM) using a FEI Quanta250 microscope. Nitrogen adsorption-desorption isotherms were measured in ASAP2020 adsorption analyzers (Micrometrics) at −196 °C. Samples were previously outgassed at 250 °C for 12 h under vacuum. The specific surface area was calculated according to Brunauer-Emmet-Teller (BET) method. The pore size distribution (PSD) was determined from the N_2 isotherm by 2D-NLDFT heterogeneous surface mode using the SAIEUS software. X-ray diffraction (XRD) patters were recorded on a Bruker D8 Discover X-ray diffractometer, using $\lambda_{Cu\text{-}Ka}$ = 1.54056 Å radiation in the 2Θ range from 15° to 80° with a step width of 0.0198°. Raman spectra were recorded with a Renishaw spectrometer (Nanonics Multiview 2000) operating with an excitation wave-length of 532 nm. The spectra were acquired with 10 s of exposition time of the laser beam to the sample. LiPS dissolution was prepared by adding stoichiometric amounts of S_8 and Li_2S to 1,2-dimethoxyethane (DME, anhydrous, Sigma-Aldrich) solvent to obtain a final concentration of 3 mM Li_2S_6. LiPS adsorption test was done by adding 10 mg of each AC to 2 mL of aforementioned dissolution. This

combination of LiPS concentration and AC amount was found to provide the most visible results. After a few minutes, the carbons settled at the bottom of the vials and color changes in the solution were easily noticed.

Electrochemical testing: CR2032 coin cells were assembled in an argon-filled glove box using the as-described AC/sulfur composites as working electrodes, a Celgard® 1208 separator and a 14 mm diameter lithium metal chip (China Energy Lithium Co.) as counter and reference electrode. For pouch cell measurements, lithium foil of 39×55 mm and Celgard® 2325 separator were used. The electrolyte employed was a 0.5 M lithium bis-(trifluoromethanesulfonyl) imide (LiTFSI, 99.9 wt.%, Solvionic) and 0.5 M lithium nitrate ($LiNO_3$ 99.99 wt.%, Sigma-Aldrich) solution in a 1:1 (v./v.) mixture of DME and dimethyl 1,3-dioxolane (DOL). A sulfur:electrolyte ratio of 1:7 $\mu L\,mg_S^{-1}$ was fixed. Medium loading cells were subjected to various discharge and charge rates (i.e., C/20, C/10, C/5 and C/2), while high loading cells were subjected to long-life tests at C/20 and C/10. The galvanostatic measurements were performed using a Maccor Battery Tester, between 2.6 and 1.7 V.

After testing, cycled-cathodes were analyzed by SEM imaging. For this purpose, the cells were opened in an argon-filled glove box and the cathodes were gently rinsed with DME and dried. An airtight holder was employed to avoid exposure to atmosphere during transfer.

Acknowledgements

This project has received funding from the European Union's Horizon 2020 research and innovation programme Graphene Flagship Core Project 3 (GrapheneCore3) under grant agreement 881603. This work is also supported by Ministerio de Ciencia, Innovación y Universidades (MCIU), Agencia Estatal de Investigación (AEI) and the European Regional Development Fund (ERDF) (RTI2018-098301-B-I00). J. C. is a beneficiary of the Predoctoral Program from the Education Department of the Basque Government. J. L. G. U. is very thankful to the Spanish Ministry of Universities for the FPU grant [16/03498]. We are also very grateful to María Jauregui and Maria Echeverria for their assistance with XRD and SEM measurements. Finally, we want to acknowledge the company GRAPHENEA for supplying the graphene oxide used in this work.

Conflict of Interest

The authors declare no conflict of interest.

Data Availability Statement

The data that support the findings of this study are available from the corresponding author upon reasonable request.

Keywords: electrochemistry · energy storage · graphene · lithium-sulfur battery · pouch cell

[1] M. Armand, J.-M. Tarascon, *Nature* **2008**, *451*, 652–657.
[2] F. Duffner, N. Kronemeyer, J. Tübke, J. Leker, M. Winter, R. Schmuch, *Nat. Energy* **2021**, *6*, 123–134.
[3] X. Judez, G. G. Eshetu, C. Li, L. M. Rodriguez-Martinez, H. Zhang, M. Armand, *Joule* **2018**, *2*, 2208–2224.
[4] R. Borah, F. R. Hughson, J. Johnston, T. Nann, *Mater. Today* **2020**, *6*, 100046.
[5] M. Zhao, B. Q. Li, X. Q. Zhang, J. Q. Huang, Q. Zhang, *ACS Cent. Sci.* **2020**, *6*, 1095–1104.
[6] M. Rana, S. A. Ahad, M. Li, B. Luo, L. Wang, I. Gentle, R. Knibbe, *Energy Storage Mater.* **2019**, *18*, 289–310.
[7] M. R. Kaiser, S. Chou, H. Liu, S. Dou, C. Wang, J. Wang, *Adv. Mater.* **2017**, *29*, 1700449.
[8] T. Cleaver, P. Kovacik, M. Marinescu, T. Zhang, G. Offer, *J. Electrochem. Soc.* **2018**, *165*, A6029–A6033.
[9] J. L. Gómez-Urbano, J. L. Gómez-Cámer, C. Botas, N. Díez, J. M. López del Amo, L. M. Rodríguez-Martinez, D. Carriazo, T. Rojo, *Carbon.* **2018**, *139*, 226–233.
[10] S. Li, B. Jin, X. Zhai, H. Li, Q. Jiang, *ChemistrySelect* **2018**, *3*, 2245–2260.
[11] M. Wang, X. Xia, Y. Zhong, J. Wu, R. Xu, Z. Yao, D. Wang, W. Tang, X. Wang, J. Tu, *Chem. A Eur. J.* **2019**, *25*, 3710–3725.
[12] Z. Guo, B. Zhang, D. Li, T. Zhao, P. R. Coxon, C. J. Harris, R. Hao, Y. Liu, K. Xi, X. Li, *Electrochim. Acta* **2017**, *230*, 181–188.
[13] C. Barchasz, F. Mesguich, J. Dijon, J.-C. Leprêtre, S. Patoux, F. Alloin, *J. Power Sources* **2012**, *211*, 19–26.
[14] C. Kensy, P. Härtel, J. Maschita, S. Dörfler, B. Schumm, T. Abendroth, H. Althues, B. V. Lotsch, S. Kaskel, *Carbon.* **2020**, *161*, 190–197.
[15] L. Peng, G. Liu, Y. Wang, Z. Xu, H. Liu, *J. Solid State Electrochem.* **2014**, *18*, 935–940.
[16] Y. Yan, Y. Yin, Y. Guo, L.-J. Wan, *Sci. China Chem.* **2014**, *57*, 1564–1569.
[17] A. Jozwiuk, H. Sommer, J. Janek, T. Brezesinski, *J. Power Sources* **2015**, *296*, 454–461.
[18] T. Liu, H. Hu, X. Ding, H. Yuan, C. Jin, J. Nai, Y. Liu, Y. Wang, Y. Wan, X. Tao, *Energy Storage Mater.* **2020**, *30*, 346–366.
[19] L. Zhang, Y. Wang, Z. Niu, J. Chen, *Carbon* **2019**, *141*, 400–416.
[20] J. L. Gómez-Urbano, J. L. Gómez-Cámer, C. Botas, T. Rojo, D. Carriazo, *J. Power Sources* **2019**, *412*, 408–415.
[21] J. L. Gómez-Urbano, G. Moreno-Fernández, M. Arnaiz, J. Ajuria, T. Rojo, D. Carriazo, *Carbon.* **2020**, *162*, 273–282.
[22] G. Moreno-Fernández, J. L. Gómez-Urbano, M. Enterría, T. Rojo, D. Carriazo, *J. Mater. Chem. A* **2019**, *7*, 14646–14655.
[23] M. Thommes, K. Kaneko, A. V. Neimark, J. P. Olivier, F. Rodriguez-Reinoso, J. Rouquerol, K. S. W. Sing, *Pure Appl. Chem.* **2015**, *87*, 1051–1069.
[24] S. Yurdakal, C. Garlisi, L. Özcan, M. Bellardita, G. Palmisano, in *Heterog. Photocatal.*, Elsevier, **2019**, pp. 87–152.
[25] X. Liu, K. Zhu, J. Tian, Q. Tang, Z. Shan, *J. Solid State Electrochem.* **2014**, *18*, 2077–2085.
[26] M. Xue, C. Chen, Y. Tan, Z. Ren, B. Li, C. Zhang, *J. Mater. Sci.* **2018**, *53*, 11062–11077.
[27] Q. Zeng, D. W. Wang, K. H. Wu, Y. Li, F. Condi De Godoi, I. R. Gentle, *J. Mater. Chem. A* **2014**, *2*, 6439–6447.
[28] X. Yang, W. Zhu, G. Cao, X. Zhao, *RSC Adv.* **2016**, *6*, 7159–7171.
[29] A. Benítez, M. González-Tejero, Á. Caballero, J. Morales, *Materials (Basel).* **2018**, *11*, 1428.
[30] X. B. Cheng, C. Yan, J. Q. Huang, P. Li, L. Zhu, L. Zhao, Y. Zhang, W. Zhu, S. T. Yang, Q. Zhang, *Energy Storage Mater.* **2017**, *6*, 18–25.
[31] C. Yan, X. Q. Zhang, J. Q. Huang, Q. Liu, Q. Zhang, *Trends Chem.* **2019**, *1*, 693–704.
[32] C. Bi, M. Zhao, L. Hou, Z. Chen, X. Zhang, B. Li, H. Yuan, J. Huang, *Adv. Sci.* **2021**, *2103910*, 2103910.

Manuscript received: April 6, 2022
Revised manuscript received: May 2, 2022
Version of record online: May 18, 2022